2013 IEEE/RSJ International Conference on
Intelligent Robots and Systems (IROS)
November 3-7, 2013. Tokyo, Japan

Cell Patterning with Robotically Controlled Optical Tweezers

Xiao Yan and Dong Sun

Abstract—**This paper presents the use of robotically controlled optical tweezers to manipulate a group of cells into a region of interest to form the required pattern. A novel multilevel-based topology is designed to present different cell patterns in the region of interest. A potential function-based controller is developed to control the cells to form the required pattern. A pattern regulatory control force is developed which particularly addresses the special case when cells stop at undesired positions. The system stability is analyzed using Lyapunov approach. Experiment is performed with robotically controller optical tweezers to demonstrate the effectiveness of the proposed approach.**

I. Introduction

Cell patterning, which is to arrange cells at desired positions, has been a heated research topic recently due to its importance in biomedical applications, including stem cell differentiation [1]-[3], tissue engineering [4] and biosensors [5]. Appropriate control of the contact area in co-culture, cell patterning can be used to manipulate cell-cell interactions. Cell patterning could also be applied to investigate cell-ECM interactions which are critical determining cell fate of many cell types [6]-[8]. Recent studies on single cells [9]-[11] have also shown the requirements of accurate cell manipulations and positions of single cells within various microenvironments, in which cell patterning technique also plays a central role.

Many different techniques have been developed for cell patterning, such as photolithography, soft lithography, dielectrophoresis (DEP), and optical tweezers. Photolithography [12] has been widely used to pattern biological molecules and cells thanks to its high resolution. However, the restrictions on photolithographic equipments such as clean rooms and the requirements of stamps and molds make it inconvenient. Furthermore, photolithography is not suitable for patterning non-planar substrates [13]. Soft lithography [13], a non-photolithographic microfabrication technology, uses elastomeric materials to produce stamps and channels that transfer the pattern. It is relatively simpler and cheaper compared with the photolithographic technique. The disadvantage of soft lithography is that the stamps are subject to distortion of the features since the materials are all elastomeric, and some of them are not stable to many organic solvents or at high temperatures such as the PDMS-based stamps [14]. The above two cell patterning methods are ideally used to handle adherent cells only.

This work was supported in part by a grant from Research Grants Council of the Hong Kong Special Administrative Region, China (Reference no. CityU 119612), and UGC Special Equipment Grant [SEG_CityU01].

The authors are with the Department of Mechanical and Biomedical Engineering, City University of Hong Kong, Kowloon, Hong Kong (E-mail: xiaoyan2-c@my.cityu.edu.hk, medsun@cityu.edu.hk).

The DEP method [15]-[17] uses non-uniform AC electric fields to generate forces that can position cells stably. This non-contact cell manipulation approach is simple and useful, and could be applied not only in cell patterning, but also in cell sorting and separation [15]. The main disadvantage of the DEP method is that it is difficult to manipulate several target cells individually and selectively. Moreover, the voltage imposed on cells may damage the cells during the manipulation process.

Optical tweezers exhibits many advantages over aforementioned approaches for cell manipulations [18]-[26]. Optical tweezers can generate trapping forces with a strongly focused light beam, which can further trap and transport a microparticle to the desired positions precisely in a non-contact manner. Various control methods have been introduced recently for optical cell manipulation and cell patterning. A closed-loop controller was proposed in [18] to improve the robustness, resolution, and repeatability in automated transportation of multiple biological cells. In [20], path planning was taken into consideration for transporting multiple microparticles with optical tweezers, such that the target microparticles could be manipulated to the predefined goal positions with minimum time. A region-based controller was developed in [23] to manipulate single cell to a desired region which could be dynamically changing in order to fulfill task specifications. An automated arraying approach was proposed in [24] to locate microparticles groups into a predefined array with appropriate pairings using optical tweezers. Parallel teleoperation was recently introduced in [26] with multi-touch user interface to improve the manipulability of micromanipulation. This method could manipulate up to 10 particles simultaneously by fingers.

Although cells could be manipulated with high precision using optical tweezers, cell patterning should be designed with great caution as the cell positions on substrate are crucial and will affect cell spreading and differentiation. In this paper, we use robotically controlled optical tweezers to control cell patterning. In our approach, a region of interest is firstly defined for coarse cell manipulation. After locating the cells within the defined region, we further position the cells to follow the desired pattern precisely. In this paper, we introduce a multilevel-based topology that can be used to produce various cell patterns specified by the task requirements. The cells will stay with the desired pattern rather than in random positions. A pattern controller is developed to move the cells into the region to form the desired pattern in a level-by-level manner. With the proposed approach, we could achieve simultaneous manipulation of multiple microparticles, and construct different cell patterns, such that further biomedical analysis could be carried out including single cell analysis, cell differentiation, cell fusion and etc.

II. MULTILEVEL-BASED TOPOLOGY

To control a large group of cells to form the desired pattern, the cells are driven into a region of interest first. Such a region can be defined in a similar way to [23]. Suppose that the region comprises different constraint regions that can form different shapes. The *l*-th constraint region Ω_l is defined as:

$$\Omega_l : \{g_l(\Delta q_{iol}) \le 0\},$$

where $\Delta q_{iol} = q_i - q_{ol}$, $q_{ol} = [x_{ol}, y_{ol}]^T \in \mathbb{R}^2$ is a reference point within Ω_l. l is the index of the constraint region, and there are m constraint regions in total. $q_i = [x_i, y_i]^T \in \mathbb{R}^2$ is defined as the center position of the *i*-th cell from a total of n cells. If $q_i \in \Omega_l$, then the *i*-th cell is either inside or on the boundary of Ω_l.

The region Ω_I is subject to m constraint regions, and can be defined as follows:

$$\Omega_I : \{[g_1(\Delta q_{io1}), g_2(\Delta q_{io2}), \ldots, g_m(\Delta q_{iom})]^T \le 0\}.$$

It should be noted that all the cells are either inside or on the boundary of Ω_I when $q_i \in \Omega_I$. For example, a circular region of interest can be defined as follows:

$$\Omega_I : \{g_1(\Delta q_{io1}) = (x_i - x_{o1})^2 + (y_i - y_{o1})^2 - 0.25 d_1^2 \le 0\},$$

where $q_{o1} = [x_{o1}, y_{o1}]^T$ and d_1 denote the center and the diameter of the circular region of interest, respectively.

We propose a multilevel-based topology to enable the cells to form the required pattern. Similar idea was proposed in our previous work on multirobot systems [27]. The topology center is defined as $q_c = [x_c, y_c]^T \in \mathbb{R}^2$, as indicated by the "+" symbol in Fig. 1. We consider the cells to be identical. In Fig. 1, each circle represents a cell with a safety radius *R*, which is little larger than the cell radius so that the cells do not adhere with each another during the manipulation process.

Motivated by the hexagonal close-packing of atoms (hcp) in a crystal structure [28], the multilevel-based topology was initially introduced in our recent paper on shape control of robot swarms [27]. As shown in Fig. 1, the cells stay together with respect to q_c in a level-by-level structure. The level is defined as L_k, where $k = 1,2,3,...$ is the index of a level. Once the cells enter Ω_I, they will start to converge to L_1. When a level L_k is filled with cells, the remaining cells are manipulated to the next level L_{k+1}. As a result, the cells can stay together in the region of interest while forming a desired pattern on a level-by-level basis. There is no limitation on the number of cells as the multilevel-based topology can grow outwards when the number of cells increases. This level-by-level topology is the most efficient structure for cell groups to stay together as tightly as possible. As shown in Fig. 1, L_1 is located precisely at q_c, and each circle is tangent to its neighbors. This hexagonal structure has the minimal surface free energy when morphogenetic processes takes place which organizes the interommatidial precursor cells of the Drosophila pupal eye [29].

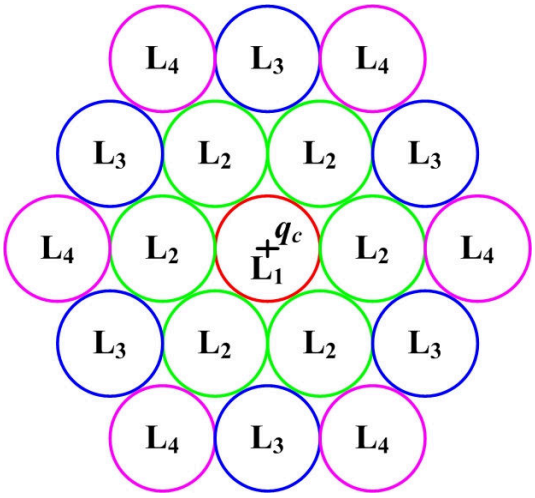

Fig. 1. Multilevel-based topology

Many different patterns can be constructed by allocating cells at different positions of different levels. Each position does not necessarily have to be filled. Based on the task requirements, the positions where cells are forbidden to go are defined as "not-to-go" positions, and further considered as "fixed obstacles" such that the cells will avoid during its movement. Hence the cells can only stop at the allowed positions as required by the desired pattern. To construct a hexagon as seen in Fig. 2, the position on L_1 is considered as a "not-to-go" position which is further considered as the "fixed obstacle". The cells are only allowed to go to the positions in solid lines on L_2 to form a hexagon within Ω_I.

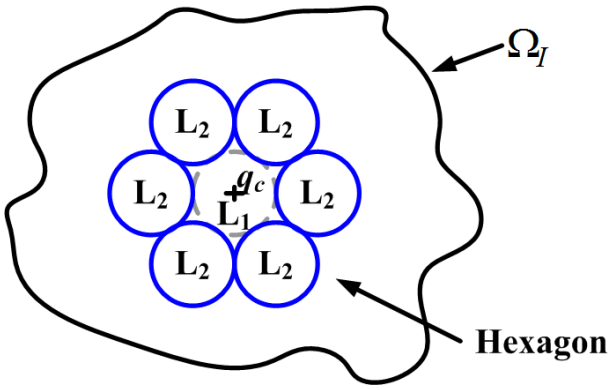

Fig. 2. Topology for a hexagon within Ω_I

III. CONTROLLER DESIGN

Consider a group of n cells and define $u_i \in \mathbb{R}^2$ as the control input for the *i*-th cell, which is the center position of the *i*-th optical trap. The dynamics of the *i*-th biological cell can be described as follows [24]:

$$m_i \ddot{q}_i = F_{trap} - F_{drag} = a_i(u_i - q_i) - b_i \dot{q}_i \qquad (1)$$

where m_i is the mass of the *i*-th cell, F_{trap} denotes the trapping force produced by the optical tweezers, which can be approximated as $a_i(u_i - q_i)$, where a_i is the trapping stiffness and $u_i - q_i$ is the offset between the optical trap center and the trapped cell center. F_{drag} represents the Stoke's drag force, where $b_i = 6\pi\mu r_i$, μ is the dynamic viscosity, and r_i is the radius of the *i*-th cell .

A. Region Control

With the proposed control approach, the cells firstly move into Ω_I and then arrive in their desired levels without collisions. Several potential field-based functions are defined to achieve the control goal.

First, the potential field of the region Ω_I can be defined as follows:

$$V_{ri}(q_i) = \frac{k_l}{2}\sum_{l=1}^{m}\left[\max\left(0, g_l(\Delta q_{iol})\right)\right]^2 \tag{2}$$

where k_l is a positive control gain for the *l*-th constraint region.

Differentiating (2) with respect to q_i yields the following potential force:

$$f_{ri} = -\nabla_{q_i} V_{ri}(q_i) \tag{3}$$

The force f_{ri} is activated to drive the cells outside to move into Ω_I. If the *i*-th cell is inside Ω_I, then $f_{ri} = 0$.

If the cells are located within Ω_I, the second force f_{ci} is generated to make the cells move toward the desired levels. The potential field $V_{ci}(q_i)$ and the corresponding force f_{ci} are designed respectively as follows:

$$V_{ci}(q_i) = \frac{1}{2}k_c(d_{ic} - R_i)^2 \tag{4}$$

$$f_{ci} = -\nabla_{q_i} V_{ci}(q_i) \tag{5}$$

where k_c is a positive control gain, R_i is the radius of the desired level of the *i*-th cell that is centered at q_c, and $d_{ic} = \|q_i - q_c\|$ denotes the distance between the *i*-th cell and the center q_c.

Mutual collisions among the cells can be avoided by designing the third force as follows:

$$f_{ij} = -\nabla_{q_i} V_{ij}(q_i, q_j) \tag{6}$$

where

$$V_{ij}(q_i, q_j) = \begin{cases} \frac{1}{2}k_{ij}(d_{ij} - 2R)^2, & if \ \ (d_{ij} < 2R, and \ L^i \geq L^j) \\ 0, & otherwise \end{cases} \tag{7}$$

where k_{ij} is a positive control gain, $d_{ij} = \|q_i - q_j\|$ is the distance between cell *i* and cell *j*, and L^i and L^j are the desired levels for the *i*-th and *j*-th cells, respectively. If the distance between cell *i* and cell *j* is less than $2R$ and $L^i \geq L^j$, then f_{ij} is activated to ensure that *i*-th cell avoids the *j*-th cell. The cells (cell *j*) that are already located at their desired levels should have higher priority to stay at the current level compared with those arriving later (cell *i*) to preserve the previously formed pattern.

Finally, a control law that combines all the three aforementioned forces is designed as follows for the *i*-th cell:

$$u_i = f_{ri} + f_{ci} + \sum_{j=1; j\neq i}^{n} f_{ij} - k_d \dot{q}_i + q_i \tag{8}$$

where k_d is a positive control gain for damping.

Theorem 1: A group of *n* cells with dynamics (1) is considered. $\dot{q}_i$ and f_{ri} converge to zero under the proposed controller (8), namely, $\dot{q}_i \to 0$ and $f_{ri} = 0$ as $t \to \infty$ for all cells.

Proof: A Lyapunov candidate function is designed as follows:

$$V(q) = \sum_{i=1}^{n}\left[V_{ri}(q_i) + V_{ci}(q_i) + \sum_{j=1, j\neq i}^{n} V_{ij}(q_i, q_j) + \frac{m_i}{2a_i}\dot{q}_i{}^T\dot{q}_i\right] \tag{9}$$

According to equations (2), (4), and (6), $V_{ri}(q_i)$, $V_{ci}(q_i)$, and $V_{ij}(q_i, q_j)$ are non-negative, and thus, $V(q) \geq 0$.

Substituting the controller (8) into (1) yields the following closed-loop equation:

$$\ddot{q}_i = \frac{a_i}{m_i}\left[f_{ri} + f_{ci} + \sum_{j=1; j\neq i}^{n} f_{ij} - \left(k_d + \frac{b_i}{a_i}\right)\dot{q}_i\right] \tag{10}$$

Differentiating (9) with respect to time yields the following:

$$\dot{V}(q) = \sum_{i=1}^{n}\dot{q}_i{}^T\left[\nabla_{q_i}V_{ri}(q_i) + \nabla_{q_i}V_{ci}(q_i) + \sum_{j=1, j\neq i}^{n}\nabla_{q_i}V_{ij}(q_i, q_j) + \frac{m_i}{a_i}\ddot{q}_i\right] \tag{11}$$

Substituting Equation (10) into Equation (11) by using Equations (2)–(7) yields the following:

$$\dot{V}(q) = -\sum_{i=1}^{n}\left(k_d + \frac{b_i}{a_i}\right)\dot{q}_i{}^T\dot{q}_i \leq 0 \tag{12}$$

Therefore, as $t \to \infty$, $\dot{q}_i \to 0$ for all cells, and so is $\ddot{q}_i$. If $f_{ri} \neq 0$, then some cells are outside Ω_I, and thus, $V_{ri}(q_i) > 0$ for such cells. These cells will then move toward Ω_I under f_{ri}, resulting in $\dot{q}_i \neq 0$, which contradicts with the conclusion that $\dot{q}_i = 0$ for all cells. Therefore, $f_{ri} = 0$. The proof is complete.

■

Using controller (8), the cells move toward the region of interest Ω_I and stop at the equilibrium state. However, controller (8) does not guarantee that all the cells are at their desired levels as required by the patterning task. In the next subsection, a pattern regulatory control force will be designed and subsequently added to controller (8) for patterning control.

B. Pattern Regulatory Control Force

In the equilibrium state, $\dot{q}_i = \ddot{q}_i = 0$, and eq. (10) can be rewritten as follows:

$$f_{ri} + f_{ci} + \sum_{j=1; j\neq i}^{n} f_{ij} = 0 \tag{13}$$

According to Theorem 1, substituting $f_{ri} = 0$ into (13) yields the following equation:

$$f_{ci} + \sum_{j=1; j\neq i}^{n} f_{ij} = 0 \tag{14}$$

It can be seen from (14) that, when $f_{ci} = 0$, $\sum_{j=1; j\neq i}^{n} f_{ij} = 0$, indicating that all the cells are located at their desired levels within Ω_I. However, when $f_{ci} \neq 0$, $\sum_{j=1; j\neq i}^{n} f_{ij} \neq 0$, indicating that f_{ci} and $\sum_{j=1; j\neq i}^{n} f_{ij}$ are equal in magnitude but with opposite directions. In such special case, the cells stop at the undesired positions, as shown in Fig. 3, a cell tries to converge to its desired level L_3, but stops at an undesired position because the two forces in (14) cancel each other. Thus, this cell stops in equilibrium state and stays at an undesired position.

Such problem can be solved by adding a pattern regulatory control force f_{si} into the controller as follows:

$$u_i = f_{ri} + f_{ci} + \sum_{j=1; j\neq i}^{n} f_{ij} + f_{si} - k_d \dot{q}_i + q_i \tag{15}$$

where

$$f_{si} = k_s T_R \frac{(q_i - q_r)}{d_{ic}} \tag{16}$$

In (16), k_s is a positive gain, $T_R = \begin{bmatrix} \cos\alpha & -\sin\alpha \\ \sin\alpha & \cos\alpha \end{bmatrix}$ is a rotation matrix, $\alpha \in (0°, 90°]$ is a constant rotation angle, and $\frac{(q_i - q_r)}{d_{ic}}$ is the unit vector, where $d_{ic} = \|q_i - q_c\|$. If $d_{ic} = 0$, then the cell is on L_1, which is not a stuck situation. Therefore, $d_{ic} > 0$. As can be seen in Fig. 3, f_{si} becomes a tangent force when α is set to $90°$.

The pattern regulatory control force f_{si} functions only when a cell stops at an undesired position. If a cell stops at a position that is not on its desired level, then the cell is considered to be at an undesired position. Consequently, f_{si} should be activated to drive this cell to leave its current position in a counter-clockwise direction. During such process, the cell may push against other cells and subsequently take their positions. The other cells then repeat the same actions until all of them leave the undesired positions.

Using the proposed controller (15), the cells can be driven toward the region of interest. Then, the cells converge to their desired levels and finally form the desired pattern within the desired region.

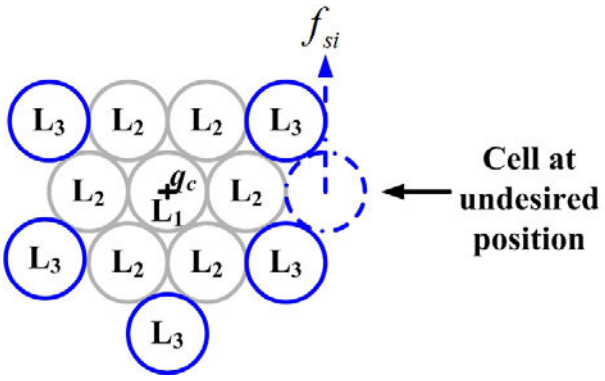

Fig. 3. Special case: cell stops at undesired position

IV. Experiments

A. Experimental Setup

Experiments were performed to demonstrate the effectiveness of the proposed control approach. Fig. 4 shows a commercially available robot-aided cell manipulation system with HOT (BioRyx 200, Arryx) that was used in the experiments. The system comprised three modules: sensory, control, and executive modules.

The sensory module is mainly used for localizing biological cells based on image processing techniques. The key components of the sensory module include a microscope (Nikon TE2000, Japan) and a CCD camera (FO124 SC, Foculus). OpenCV is used for contour detection to obtain the center position of each biological cell. The image processing technique guarantees the target cells could be trapped at all time. The control module mainly consists of a controller for the motorized stage, a phase modulator for the HOT device, and a host computer. The HOT device can generate a highly focused laser beam with the wavelength of 1064 nm (V-106 C-3000 OEM J-series, Spectra Physics). Moreover, the HOT devices can create and control multiple optical traps (up to 200) simultaneously. These traps are considered as micro end-effectors for cell manipulation in a microenvironment. The executive module consists of a motorized stage (ProScan, Prior Scientific), a HOT device, and a joystick controller. As can be seen in Fig. 4, the motorized stage can be controlled in the XY plane by using the joystick controller. Cells are placed in a chamber positioned on the motorized stage.

The actual size of each pixel on the CCD camera was approximately 0.12 μm under 60x magnification, and the camera had a resolution of 640 × 480. For successful

manipulation, the optical trap was positioned within the coordinate range (512×512) of the diffractive element device (DED). Therefore, control precision was 0.15 μm horizontally and 0.11 μm vertically [24].

B. *Experimental Results*

The maximum power of the HOT system was 3 watts. Under this power limit, the suitable number of cells under simultaneous manipulation varies for different cell types. In our experiments, yeast cells (3-4 μm on average) were used as they were easy to obtain and manipulate with optical tweezers. A circular region of interest Ω_I was defined as:

$$\Omega_I : \left\{ g_1(\Delta q_{io1}) = (x_i - x_{o1})^2 + (y_i - y_{o1})^2 - 0.25 d_1^{\,2} \le 0 \right\},$$

where $q_{o1} = [x_{o1}, y_{o1}]$ is the image center acquired from the CCD camera and $d_1 = 460$ pixels. The control parameters were set as $k_1 = 10$, $k_c = 20$, $k_{ij} = 500$, and $k_d = 1$. The safety radius R was set as $R = 36$ pixels.

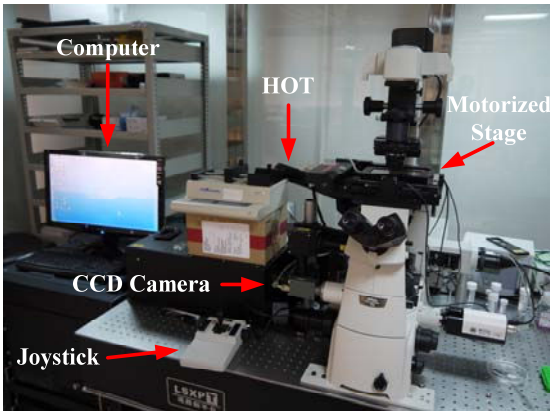

Fig. 4. Experimental setup

Each target cell was trapped and moved by one single optical trap generated by the HOT, and the sampling time of the system was set as 100 ms. The maximum velocity and acceleration of the optical tweezers were set to 80 pixels/s and 600 pixels/s^2, respectively. A higher moving velocity caused the cells to escape from the optical traps. Calibration study of the maximum moving velocity has been reported in [19].

In the experiment, six cells were manipulated using HOT to construct a hexagon inside the region of interest Ω_I. In Fig. 5, six yeast cells were initially outside Ω_I, as shown in Fig. 5(a), and then converged to Ω_I after 1 s. After 7.5 s, the cells formed a hexagonal pattern. Figs. 6 and 7 show the absolute velocity and positional error (distances to its desired level) of cell 1, respectively. As can be seen in Fig.6, cell 1 was moving in maximum speed of 80 pixels/s initially, but its speed dropped starting at $t = 2s$. The reason for this speed drop was because the cell approached to its desired level. However, the velocity of cell 1 fluctuated after 2.5 s mainly due to the interaction forces from neighboring cells. As time went on, the interaction forces from neighboring cells decreased and the speed of the cell dropped as well. As shown in Figs.6-7, the absolute velocity and absolute positional error of cell 1 both converged to 0 finally. The experimental results of other cells were similar and therefore not shown here. The sum of the absolute velocities and positional errors of all cells are shown in Fig. 8 and Fig.9, respectively.

The above experimental results demonstrate the effectiveness of the proposed cell patterning control approach. The cells were able to be manipulated towards the region firstly. After the cells were located within the region of interest, the desired pattern could be constructed finally with the proposed control approach.

V. Conclusion

This study presented a novel approach to the pattern control of biological cells in a predefined region of interest by using a robotically controlled HOT. A multilevel-based topology was introduced to define various patterns. The cells were required to form the desired pattern inside the region of interest rather than staying in random positions. A potential function-based controller with a pattern regulatory control force was developed to drive all the cells to form the desired pattern without collisions. The stability of the system was analyzed using a Lyapunov approach. Experiment was performed to demonstrate the effectiveness of the proposed approach.

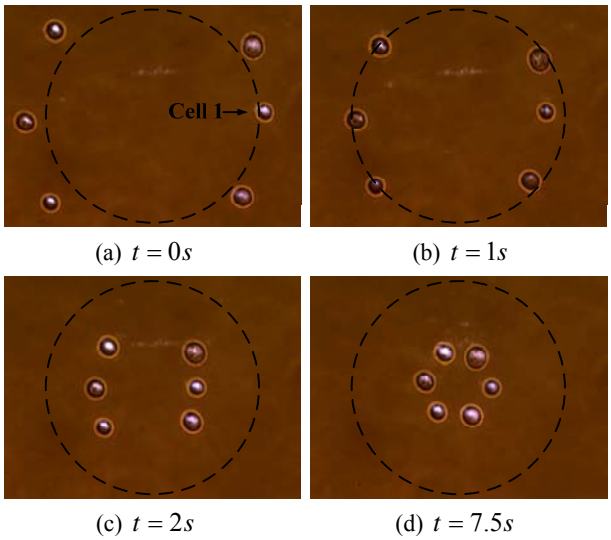

Fig. 5. Experiment results: hexagonal pattern

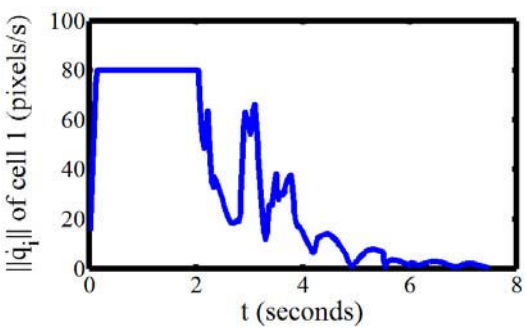

Fig. 6. Experimental result: absolute velocity of cell 1

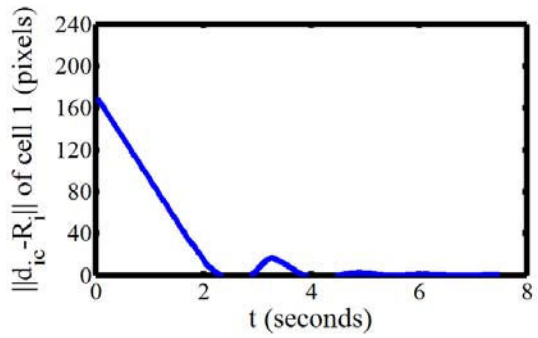

Fig. 7. Experimental result: absolute positional error of cell 1

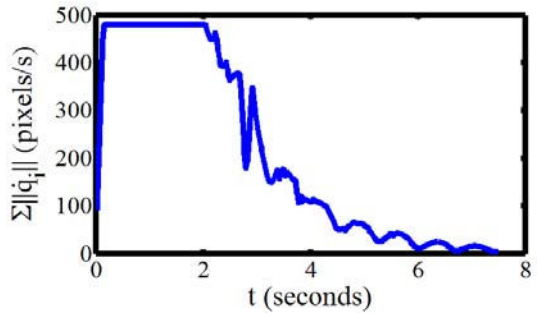

Fig. 8. Experimental result: sum of absolute velocities of all cells

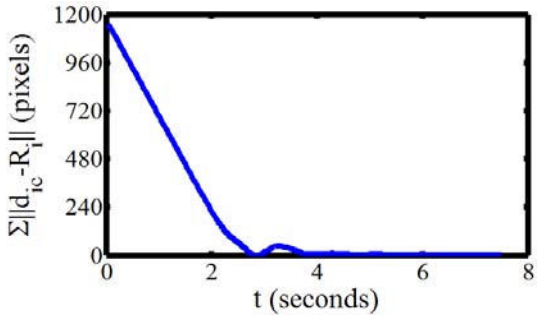

Fig. 9. Experimental result: sum of absolute positional errors of all cells

REFERENCES

[1] J. Tang, R. Peng, and J. Ding, "The regulation of stem cell differentiation by cell-cell contact on micropatterned material surfaces," *Biometerials*, 31(9), pp. 2470-2476, 2010.

[2] A. Beduer, C. Vieu, F. Arnauduc, J. Sol, I. Loubinoux, and L. Vaysse, "Engineering of adult human neural stem cells differentiation through surface micropatterning," *Biometerials*, 33(2), pp. 504-514, 2012.

[3] A. Rosenthal, A. Macdonald, and J. Voldman, "Cell Patterning Chip for Controlling the Stem Cell Microenvironment," *Biometerials*, 28(21), pp. 3208-3216, 2007.

[4] B. Guillotin, and F. Guillemot, "Cell patterning technologies for organotypic tissue fabrication," *Trends Biotechnol*, 29(4), pp. 183-190, 2011.

[5] J. El-Ali, P. K. Sorger, and K. F. Jensen, "Cells on chips," *Nature*, 442, pp. 403-411, 2006.

[6] N. F. Huang, B. Patlolla, O. Abilez, H. Sharma, J. Rajadas, R. E. Beygui, C. K. Zarins, and J. P. Cooke, "A matrix micropatterning platform for cell localization and stem cell fate determination," *Acta Biomater*, 6(12), pp. 4614-4621, 2010.

[7] B. Trappmann, J. E. Gautrot, J. T. Connelly, D. G. T. Strange, Y. Li, M. L. Oyen, M. A. Cohen Stuart, H. Boehm, B. Li,V. Vogel, J. P. Spatz, F. M. Watt, and W. T. S. Huck, "Extracellular-matrix tethering regulates stem-cell fate," *Nature Materials*, 11, pp. 642-649, 2012.

[8] C.J. Flaim, S. Chien, and S. N. Bhatia, "An extracellular matrix microarray for probing cellular differentiation," *Nat Methods*, 2(2), pp.119-125, 2005.

[9] C.E. Sims, and N.L. Allbritton, "Analysis of single mammalian cells on-chip," *Lab Chip*, 7(4), pp. 423-440, 2007.

[10] J. Zhou, Y. Wu, S. K. Lee, and R. Fan, "High-content single-cell analysis on-chip using a laser microarray scanner," *Lab Chip*, 12(23), pp. 5025-5033, 2012.

[11] D. D. Carlo, L. Y. Wu, and L. P. Lee, "Dynamic single cell culture array," *Lab Chip*, 6(11), pp. 1445-1449, 2006.

[12] N. Li, and C.M. Ho, "Photolithographic patterning of organosilane monolayer for generating large area two-dimensional B lymphocyte arrays," *Lab Chip*, 8(12), pp. 2105-2112, 2008.

[13] R. S. Kane, S. Takayama, E. Ostuni, D. E. Ingber, and G. M. Whitesides, "Patterning proteins and cells using soft lithography," *Biometerials*, 20(23-24), pp. 2363-2376, 1999.

[14] D. G. Bucknall, *Nanolithography and Patterning Techniques in Microelectonics*, Woodhead Pub, 2005.

[15] H. H. Cui, J. Voldman, X. F. He, and K. M. Lim, "Separation of particles by pulsed dielectrophoresis," *Lab Chip*, 9(16), pp. 2306-2312, 2009.

[16] L. M. Fu, G. B. Lee, Y. H. Lin, and R. J. Yang, "Manipulation of microparticles using new modes of traveling-wave-dielectrophoretic forces: numerical Simulation and experiments," *IEEE/ASME Trans. Mech.*, 9(2), pp. 377-383, 2004.

[17] H. Maruyama, K. Kotani, A. Honda, T. Takahata, and F. Arai, "Nanomanipulation of single virus using dielectrophoretic concentration on a microfluidic chip," *In Proc. IEEE Conf. Autom. Sci. Eng.*, pp. 710-715, 2010.

[18] S. Hu, and D. Sun, "Automatic transportation of biological cells with a robot-tweezer manipulation system," *Int J Robot. Res.*, 30(14), pp. 1681–1694, 2011.

[19] Y. Wu, D. Sun, W. Huang, and N. Xi, "Dynamics analysis and motion planning for automated cell transportation with optical tweezers," *IEEE/ASME Trans. Mech.*, 18(2), pp. 706-713, 2013.

[20] A. S. Banerjee, A. Pomerance, W. Losert, and S. K. Gupta, "Developing a stochastic dynamic programming framework for optical tweezer-based automated particle transport operations," *IEEE Trans. Autom. Sci. Eng.*, 7(2), pp. 218-227, 2010.

[21] X. Wang, S. Chen, M. Kong, Z. Wang, K. D. Costa, R. A. Li, and D. Sun, "Enhanced cell sorting and manipulation with combined optical tweezer and microfluidic chip technologies," *Lab Chip*, 11(21), pp. 3656-3662, 2011.

[22] S. C. Chapin, V. Germain, and E. R. Dufresne, "Automated trapping, assembly, and sorting with holographic optical tweezers," *Opt. Express*, 14(26), pp. 13095-13100, 2006.

[23] X. Li, and C.C Cheah, "Dynamic region control for robot-assisted cell manipulation using optical tweezers," *In Proc. IEEE Int. Conf. Robot. Autom.*, USA, pp. 1057-1062, 2012.

[24] H. Chen, and D. Sun, "Moving groups of microparticles into array wit h a robot-tweezers manipulation system," *IEEE Trans. Robot.*, 28(5), pp. 1069-1080, 2012.

[25] X. Wang, X. Yan, S. Chen, and D. Sun, "Automated parallel cell isolation and deposition using microwell array and optical tweezers," *In Proc. IEEE Int. Conf. Robot. Autom.*, USA , pp. 4571-4576, 2012.

[26] K. Onda, and F. Arai, "Parallel teleoperation of holographic optical tweezers using multi-touch user interface," *In Proc. IEEE Int. Conf. Robot. Autom.*, USA, pp. 1069-1074, 2012.

[27] X. Yan, J. Chen, and D. Sun, "Multilevel-based topology design and shape control of robot swarms," *Automatica*, 48(12), pp. 3122-3127, 2012.

[28] D. A. Weitz, "Packing in the spheres," *Science*, 303(5660), pp. 968-969, 2004.

[29] S. Bao, and R. Cagan, "Preferential adhesion mediated by Hibris and Roughest regulates morphogenesis and patterning in the Drosophila eye," *Dev Cell*, 8(6), pp. 925-935, 2005.